



TSUNAMI DAMAGE DETECTION USING MODERATE-RESOLUTION SATELLITE IMAGERY

F. Yamazaki¹, K. Kouchi², and M. Matsuoka³

ABSTRACT

A moment-magnitude 9.0 earthquake struck the area off the western coast of northern Sumatra on 26 December 2004, which triggered massive tsunamis inundating the coastal areas in the countries along the Indian Ocean Rim. Various moderate- to high-resolution satellite images were obtained before and after the tsunami attack and used for emergency management. High-resolution satellite (e.g. IKONOS) images allowed us to visually identify tsunami-affected areas with satisfactorily high accuracy, whereas moderate-resolution satellites (e.g. Terra-ASTER) would be more valuable for this kind of large-scale disasters. Since the change in land cover classes before and after the tsunami gave a good differentiation of tsunami inundation, multi-spectral satellite imagery is also thought to be useful to detect this change. In this study, the analysis on the thresholds of the indices to indicate surface characteristics such as the normalized difference vegetation index (NDVI), soil index (NDSI), and water index (NDWI) was carried out using moderate-resolution imagery. The thresholds were studied in two cases; one is for the tsunami damage detection based on only the data acquired after the disaster, and the other is for the detection based on the difference data of these indices before and after the tsunami.

Introduction

In the stage of emergency management after the occurrence of natural disasters, a quick response including rapid decision-making and information-gathering seems to be crucial as was shown through the experience of Hurricane Katrina in the United States in 2005. Recent advancements in remote sensing and its application technologies have made it possible to use remotely sensed imagery for capturing damage distributions due to natural disasters. Especially it is important to capture extensive damage distribution immediately after earthquakes or other disasters. For this purpose, remote sensing data is thought to perform an important role in collecting information of damage in broad areas.

Since remote sensing data observed by various sensors on board various platforms have both advantages and disadvantages in immediacy, periodicity, and resolution etc., it is necessary

¹ Professor, Faculty of Engineering, Chiba University, Chiba, Japan. Email: yamazaki@tu.chiba-u.ac.jp

² Graduate Student, Dept of Civil Engineering, The University of Tokyo, Tokyo, Japan.

³ Team Leader, Earthquake Disaster Mitigation Research Center (EDM), NIED, Kobe, Japan.

to consider the characteristics of each platform and sensor and the quality of data when they are used. In order to examine the applicability of remote sensing technologies to emergency management after earthquakes, visual damage detection was performed using aerial photographs (Ogawa and Yamazaki 2000). However, these kinds of images have critical disadvantages that are a narrow area covered with one acquisition time and restrictions of using airplanes due to regulations or topography. On the other hand, satellite images would be able to resolve these problems. As for the resolution of satellite images, it has been demonstrated that high-resolution satellite images could be applied to detecting even building damage (Yamazaki et al. 2004).

As a result of the improvement of the frequency and quality of remote sensing data, it has become possible that a large number of data acquired by satellites are provided immediately after disasters. During the 2004 Indian Ocean Tsunami, a large number of remotely sensed images before and after the tsunami were delivered under the International Charter (Oo et al. 2005) and were very useful for rescue and rehabilitation actions. Note that a dual-scale approach for detection of tsunami-affected areas using satellite images has been proposed (Vu et al. 2005).

In this paper a fundamental analysis is carried out for the purpose to develop a technique of detecting tsunami-affected areas using multi-spectral satellite imagery for the areas hit by the 2004 Indian Ocean Tsunami. Referring to the result of damage detection based on multi-temporal high-resolution images (Vibulsreth et al. 2005) as the truth data, the characteristics of affected areas and others are analyzed and compared using moderate-resolution satellite imagery.

Tsunami Damage in South Thailand

A moment-magnitude 9.0 earthquake struck the area off the western coast of northern Sumatra on 26 December 2004, which triggered massive tsunamis inundating the coastal areas in the countries along the Indian Ocean Rim. The present authors conducted a reconnaissance survey in southern Thailand in January 2005 (Yamazaki et al. 2005). The survey indicated how damaged areas looked as shown in Fig. 1. This would be valuable reference data for developing the algorithm of damage detection. From all of the survey areas, Khao Lak in Phang-Nga province, Thailand, was chosen as the study area.

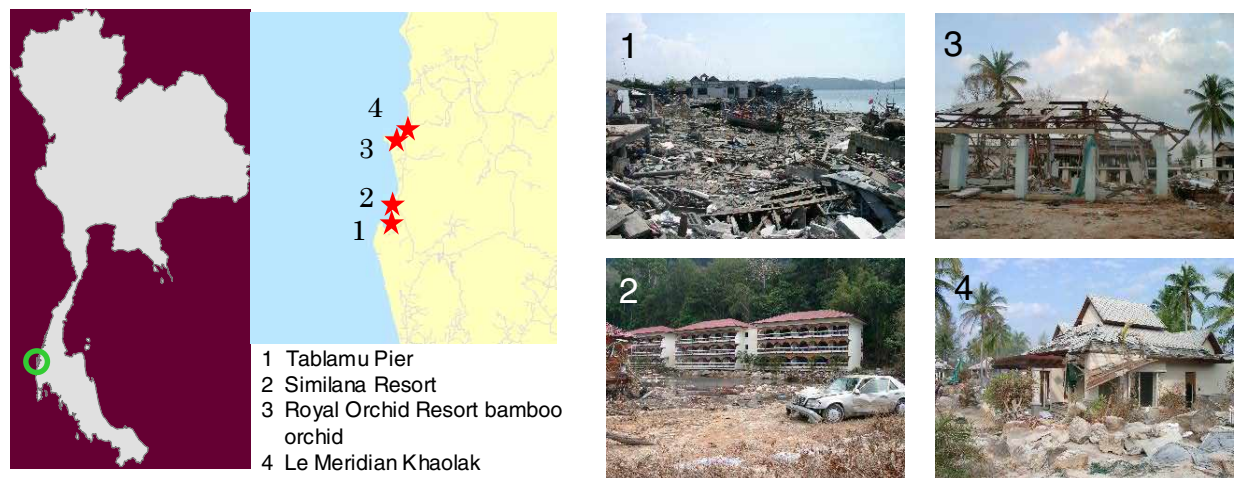


Figure 1. Photographs taken during the field survey in Phang-Nga province, Thailand.

Visual Damage Detection Using High-resolution Imagery

It is possible to identify even individual buildings in high-resolution images. Even though building damage levels judged from vertical images are tend to be estimated relatively lower than actual damage levels (Yano et al. 2004), the identification of inundation areas would be more accurate because of the extent of damage distribution. Therefore, the inundation areas extracted visually from a high-resolution image would well correspond with actual affected areas.

After the 2004 Indian Ocean tsunami, Geo-Informatics and Space Technology Development Agency (GISTDA), Thailand, monitored the tsunami disaster using various satellite images and, as a result, extracted the affected areas in the southern Thailand based on multi-temporal and multi-resolution imagery (Vibulsreth et al. 2005). Figure 2 shows the extracted areas overlaid on IKONOS image acquired on 21 April 2005, which is used as the truth data of tsunami inundation.

As is mentioned above, high-resolution images provide detailed information of damage. As well as that, because of their wide area covered at one acquisition time, moderate-resolution images are also important when it is necessary to obtain quickly the extensive information on damage distribution, which could, in particular, help emergency management such as relief logistics. In the next section, an analysis on damage detection using ASTER images about two years before and 5 days after the earthquake was performed.

Towards the Detection Using Moderate-resolution Images

ASTER images covering the same area as Fig. 2 are shown in Fig. 3. In the figure, the reflectance of the near-infrared band is assigned to the red component, that of the red band to the green component, and that of the green band to the blue component, respectively.

Comparing these images, it could be observed that the reflectance of the near-infrared band in the affected areas became weak after the tsunami, which roughly means that, due to the tsunami, vegetation there might be removed/killed and that the land cover class there might be changed to soil. This has also been confirmed in the field survey.

The ASTER sensor can collect the data of not only visible and near-infrared bands but also a short wavelength infrared band. The resolution is 15 meters for visible and near-infrared bands and 30 meters for the short wavelength infrared band. Hence, ASTER data with moderate-resolution is useful for detecting wide tsunami inundation areas quickly because red, near-infrared and short wavelength infrared bands are considered to give the good indicators of land cover characteristics and, in fact, the normalized difference vegetation, soil and water indices have been proposed using these three bands (Takeuchi and Yasuoka 2004). In the next section, these indices are computed and their characteristics in affected areas and other areas are analyzed. This would be a fundamental analysis for tsunami damage detection.

Before moving into image processing like the computation of indices, pre-processing is mandatory. Because data corrections like atmospheric correction and data conversion into reflectance were executed by the vendor, the registration of images acquired at different times and the correction of shadow and cloud areas are required.



Figure 2. Visual damage detection result based on high-resolution images (Vibulsreth et al.

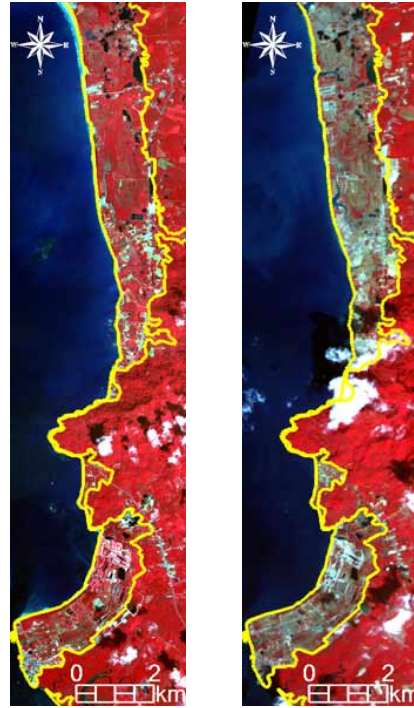


Figure 3. ASTER false color images (left:15/11/2002, right: 31/12/2004).

Registration was carried out through collecting ground control points. Then, the correction of shadow and cloud areas was performed following the flowchart shown in Fig. 4. Firstly, through maximum likelihood classification using the visible and near-infrared bands, ASTER images before and after the disaster were classified into cloud, shadow, water and earth classes etc. Secondly, the mask of the cloud class was built in order to exclude the cloud areas in subsequent image processing, while the shadow pixels were corrected in the following way. At the beginning, scanning the image from the upper-left pixel to the lower-right pixel is started in order to detect shadow pixels. When a shadow pixel is detected, the mean value of its neighboring pixels (within a 7x7 window) that have been classified into neither the shadow class, the cloud class nor the water class is calculated. Then, the pixel is replaced by that mean value. This pixel shall be used for the calculation of mean values of shadow pixels detected hereafter. After the scanning is restarted and another shadow pixel is detected, it is replaced by the mean value of the neighboring pixels. These operations are repeated to complete the correction of the shadow pixels. The result of classification and correction of shadow areas are shown in Fig. 5.

Indices of Land Cover Classes

As is mentioned above, it would be possible to identify the areas where the land cover class has changed as tsunami inundation areas. Therefore, for the purpose of demonstrating the applicability of the vegetation, soil and water indices to detecting tsunami-affected areas, these indices need to be analyzed. From the reflectance of the red (RED), near-infrared (NIR), and short wavelength bands (SWIR), the normalized difference vegetation (NDVI), soil (NDSI) and water (NDWI) indices were computed following Equations 1-3 (Takeuchi and Yasuoka 2004).

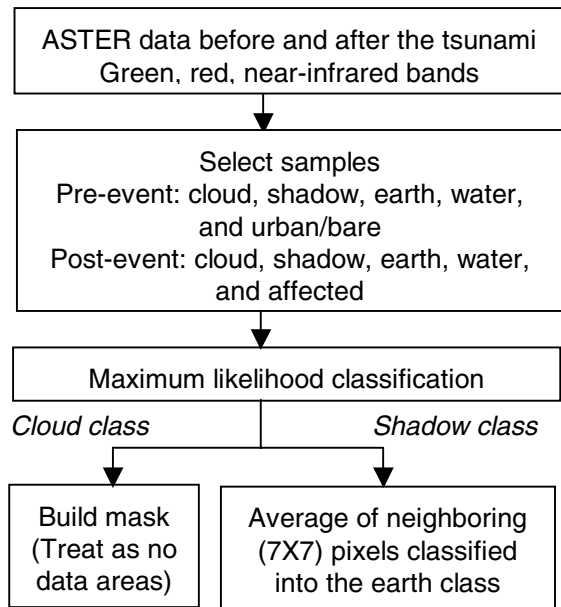


Figure 4. Flowchart of the correction of cloud and shadow areas.

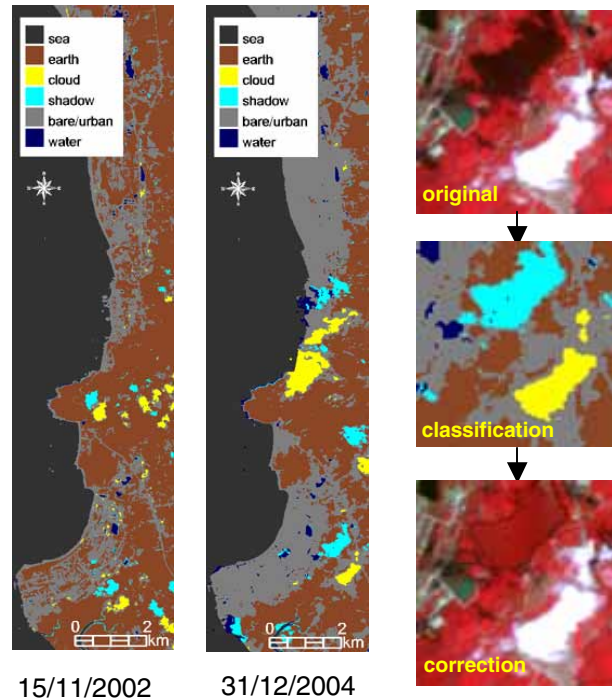


Figure 5. Classification result (yellow: cloud, cyan: shadow) and the correction of shadow areas.

$$\text{NDVI} = (\text{NIR} - \text{RED}) / (\text{NIR} + \text{RED}) \quad (1)$$

$$\text{NDSI} = (\text{SWIR} - \text{NIR}) / (\text{SWIR} + \text{NIR}) \quad (2)$$

$$\text{NDWI} = (\text{RED} - \text{SWIR}) / (\text{RED} + \text{SWIR}) \quad (3)$$

The thematic maps of NDVI, NDSI, and NDWI are shown in Fig. 6. The greater NDVI is, the more probable it is that the area is covered with vegetation. It is also the case with NDSI for soil and NDWI for water. The results demonstrate clear difference in the indices for the affected areas before and after the disaster and difference between the affected areas and the other areas after the disaster. These differences could be good indicators of tsunami inundation. Hence, the analysis on the characteristics of the indices depending on damage states is important for considering the applicability of these indices to tsunami damage detection.

Threshold Analysis on Indices to Identify Tsunami-affected Areas

For Identification Using the Data After the Tsunami

Figure 6 indicates that NDVI decreased, and NDSI and NDWI increased in the tsunami-affected areas after the disaster, as a whole. Therefore, it could be considered that, because of the tsunami, vegetation in the affected areas was washed away or dead/weakened and soil was exposed there. Moreover, the amount of water caught in and on the soil increased.

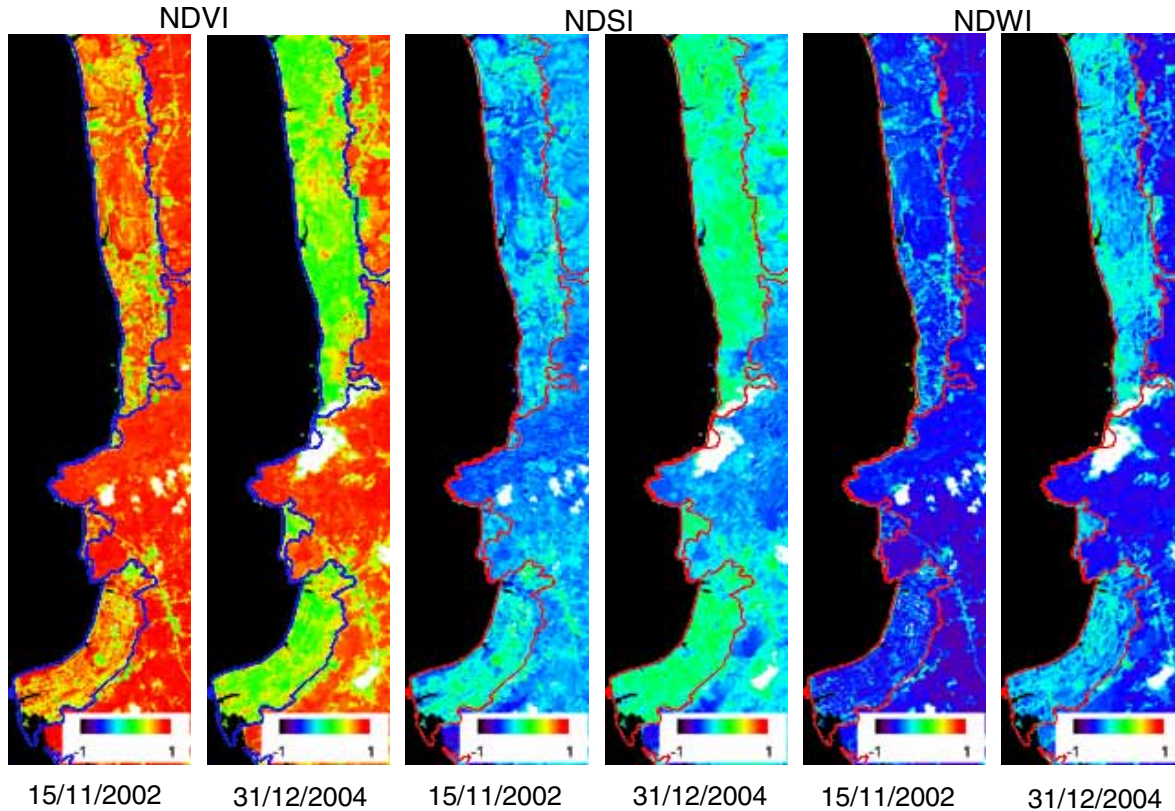


Figure 6. Thematic maps of NDVI, NDSI, and NDWI.

Obtaining the distribution of the three indices in the affected areas and the other areas from the data acquired after the tsunami, the ranges of indices that characterize the damage were calculated. The aim of this study is to determine the thresholds for detecting tsunami-affected areas using post-event data. Note that this method would be valid for only the region where there is abundance of vegetation because it is assumed that the disappearance of vegetation due to the tsunami could be detected in this method.

Based on the post-event data, the cumulative frequency distributions of NDVI, NDSI and NDWI in the affected areas and the other areas were plotted in Fig. 7. Subsequently, the points between 20 and 80 percentiles were connected by a straight line. Besides, the range that the index has in the affected area was assumed from the intersection between its extension and the 0 percent line to that between its extension and the 100 percent line. These ranges are listed in Table 1. It is proposed the technique that the pixels which have all of the indices in these ranges are identified as affected areas in tsunami damage detection using the post-event data.

In practice, the fluctuation of the indices depending on the season and the initial distribution of vegetation should be considered and corrected. Moreover, NDWI might be especially influenced by the weather condition and the time passage after the tsunami. Hence, after understanding the change of the indices in year, the thresholds calculated this time should be adjusted to reflect the seasonal characteristics and the vegetation distribution in the further study. Additionally, it has to be ensured that indices give clear difference between affected areas and other areas beforehand. It seems that an alternative solution is to use the difference of these indices between pre- and post-event data as the indicators of tsunami damage.

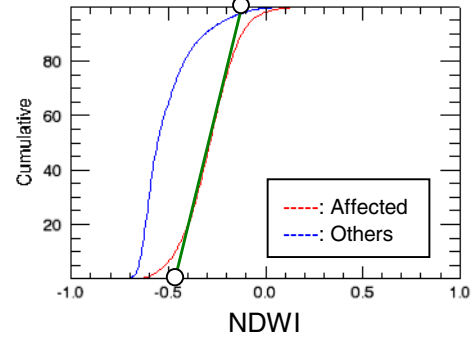
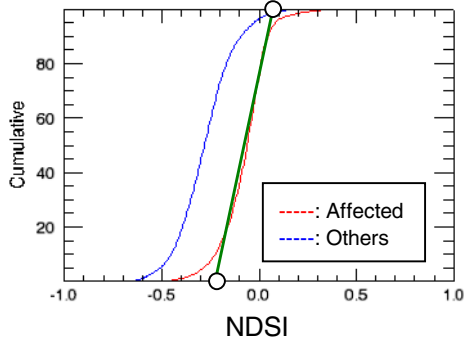
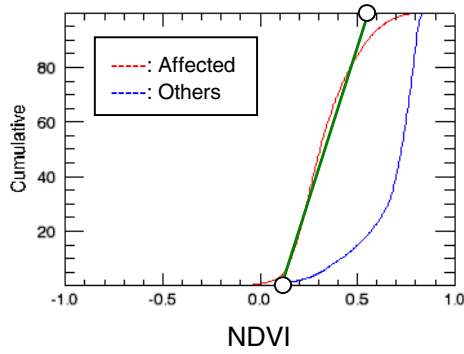


Table 1. Ranges that the indices have in the affected areas and the other areas.

	Affected		Ref. Others	
	Min (0%)	Max (100%)	Min (0%)	Max (100%)
NDVI	0.1218	0.5534	0.5000	0.8642
NDSI	-0.2124	0.0745	-0.4652	-0.0889
NDWI	-0.4645	-0.0960	-0.6796	-0.3476

Figure 7. Cumulative frequency distributions of NDVI, NDSI, and NDWI from the post-event data (red: the affected areas, blue: the other areas).

For Identification Using the Data Before and After the Tsunami

As is demonstrated above, the tsunami caused vegetation to be removed (corresponding to the NDVI decrease), soil to be exposed (the NDSI increase) and water to exist in or on the soil (the NDWI increase) after the event. Hence, it might be possible to identify the pixels where all the indices have changed significantly in the tsunami-affected areas.

Firstly, the pixels where NDVI before the tsunami is high enough to indicate the existence of vegetation were extracted and used for the subsequent operations. Hence, pixels with NDVI that is less than 20 percentile of its cumulative frequency distribution in the affected areas based on the pre-event data, 0.4801, were excluded (depicted in gray in Fig. 8). In other words, the difference of NDVI between the pre- and post-event data was computed only with the pixels where NDVI is greater than 0.4801 before the tsunami.

As for NDSI and NDWI, on the contrary, the target, which should not be classified as soil and water classes, is only the pixels where the indices are less than 80 percentile of their cumulative frequency distributions based on the pre-event data. The thresholds are summarized in Table 2. Then, only for these target pixels, the difference of each index was computed.

Secondly, after the differences of the indices between the pre- and post-event data were obtained, the differences due to the season were necessary to be subtracted. They were derived from the differences of the average for the areas without tsunami effects between the pre- and post-event data. These averages and their differences of the indices are shown in Table 3. Subtracting these values from the simple differences between the two data, the differences of the indices considering seasonal change to some extent was obtained as shown in Fig. 8.

According to these figures, rather large differences of the indices can be seen mainly in the affected areas. As well as that, some pixels where the indices, especially NDVI and NDSI, are obviously different between the pre- and post-event data are also observed in the other areas. In these areas NDVI decreased and NDSI increased. Referring to the pre- and post-event ASTER images and the post-event IKONOS image shown in Fig. 9, it can be concluded that artificial land use changes with tree cutting caused that differences in these areas. In addition, another evidence is that the edge of these areas consists of straight lines, as a whole. This discussion above indicates that multi-resolution and multi-temporal imagery are pretty helpful for understanding entities in the real world.

Lastly, the distribution of difference for the three indices in the affected areas and the other areas was calculated. Based on that, the ranges of indices' differences that characterize the damage due to the tsunami were obtained. The aim of this study is to determine the thresholds for detecting tsunami-affected areas using the difference between the pre- and post-event images.

From the difference data, the cumulative frequency distributions of the differences of NDVI, NDSI, and NDWI in the affected areas and the other areas were plotted in Fig. 10. In a similar way to the detection using only the post-event data, the ranges of indices' differences for predicting tsunami-affected areas were determined. These ranges are summarized in Table 4.

Table 2. Thresholds of the indices to determine the target pixels for computing differences of the indices between pre- and post-event data.

	Direction	Threshold
NDVI	more than	0.4802
NDSI	less than	-0.1434
NDWI	less than	-0.3371

Table 3. Average of each index for the no-damage areas and their difference between pre-event and post-event data.

	Areas without tsunami damage		
	Pre-event	Post-event	Difference
NDVI	0.7545	0.6721	-0.0824
NDSI	-0.3390	-0.2732	0.0658
NDWI	-0.5730	-0.5057	0.0673



Figure 9. ASTER and IKONOS images of the area where land use was changed artificially.

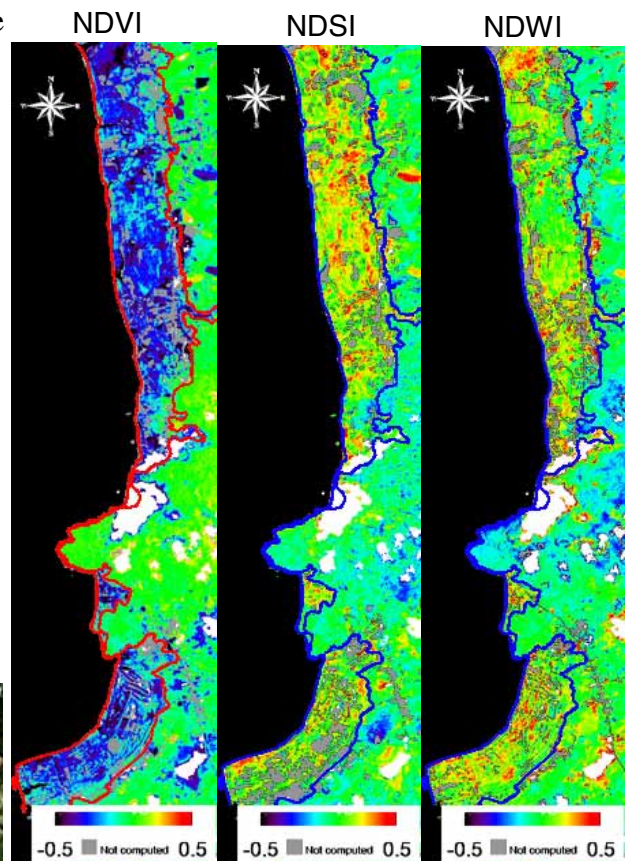


Figure 8. Differences of the indices between the pre- and post-event data.

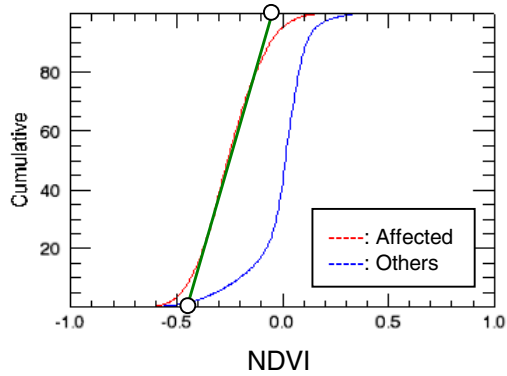


Table 4. Ranges that indices' differences have in the affected areas and the other areas.

	Affected		Ref. Others	
	Min (0%)	Max (100%)	Min (0%)	Max (100%)
NDVI	-0.4519	-0.0398	-0.1243	0.1332
NDSI	-0.0039	0.3324	-0.1239	0.1285
	→ 0			
NDWI	-0.0308	0.3266	-0.1494	0.1591
	→ 0			

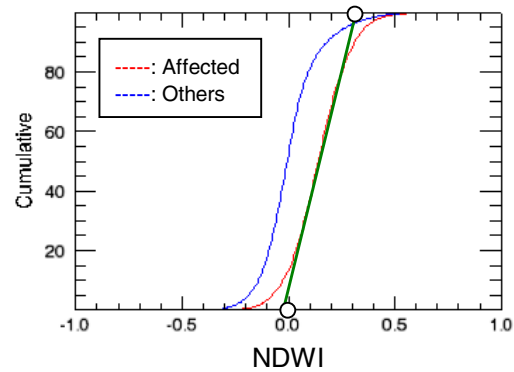
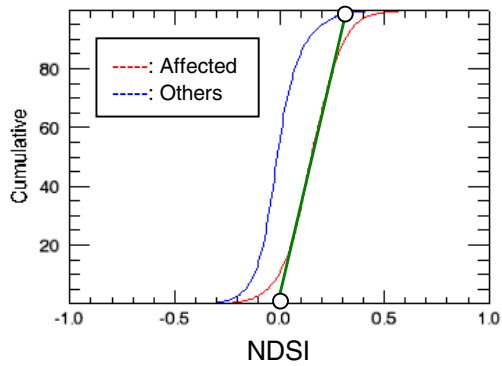


Figure 10. Cumulative frequency distributions of the differences of NDVI, NDSI, and NDWI (red: the affected areas, blue: the other areas).

Here, the minimum values of the ranges for NDSI difference and NDWI difference, which were negative values, were revised and changed into zero because it was assumed that, in principle, NDSI and NDWI would increase in the tsunami-affected areas after the tsunami. It is proposed the technique that the pixels which have all of the indices' differences in these ranges shown in Table 4 are identified as tsunami-affected areas in tsunami damage detection based on pre- and post-event images.

Although it is considered that there could be little dependence of these ranges on the initial distribution of vegetation in the site by using only pixels with high NDVI, it is still necessary to define the threshold to extract the pixels where NDVI is high enough to indicate the existence of vegetation, which would be influenced by the season and the vegetation distribution.

Conclusions

In this paper the fundamental analysis towards tsunami-damage detection techniques using moderate-resolution satellite imagery for the areas hit by the 2004 Indian Ocean Tsunami was carried out. Focusing on land cover change due to the tsunami, three indices to indicate land cover characteristics, which are NDVI, NDSI, and NDWI, were employed in order to detect the areas affected by the tsunami. Through the analysis on these indices, it has been demonstrated that, as a whole, the tsunami caused the decrease of NDVI and the increase of NDSI and NDWI.

First, the ranges which the indices in the tsunami-affected areas would have been calculated using only the post-event image. It is considered that the pixels which have all of the indices in these ranges could be identified as tsunami-affected areas in tsunami damage detection using only the post-event image. Next, for the purpose of clearing the fluctuation of the indices depending on seasons, the differences of the indices between the pre- and post-event images were computed. Then, in the same way, the thresholds of the indices' differences were considered in order to detect affected areas.

In the future study, it is necessary to demonstrate the applicability of the thresholds obtained in this paper by applying these values to the multi-level slice technique and evaluating the accuracy of damage detection based on truth data.

Acknowledgments

The visual detection result of tsunami-affected areas based on IKONOS images were provided by Ms. Supapis Polngam, GISTDA, Thailand.

References

- Ogawa, N., and Yamazaki, F., 2000. Photo-Interpretation of Building Damage due to Earthquakes Using Aerial Photographs, *Proceedings of the 12th World Conference on Earthquake Engineering*, CD-ROM, Paper No. 1906, 8p.
- Oo, K., S., Mehdiyev, M., and Samarakoon, L., 2005. Potential of Satellite Data in Assessing Coastal Damage Caused by South-Asia Tsunami in December 2005 – A Field Survey Report, *Asian Journal of Geoinformatics*, Vol. 5, No. 2, pp. 16-37.
- Takeuchi, W., and Yasuoka, Y., 2004. Development of normalized vegetation, soil and water indices derived from satellite remote sensing data, *Journal of the Japan Society of Photogrammetry and Remote Sensing*, Vol. 43, No. 6, pp. 7-19 (in Japanese).
- Vibulsreth, S., Ratanasermping, and S., Polngam, S., 2005. Tsunami Disasters along the Andaman Sea, Thailand, *Asian Journal of Geoinformatics*, Vol. 5, No. 2, pp. 3-15.
- Vu, T., T., Matsuoka, M., and Yamazaki, F., 2005. Dual-scale approach for detection of tsunami-affected areas using optical satellite images, Submitted to *International Journal of Remote Sensing*.
- Yamazaki, F., Kouchi, K., Matsuoka, M., Kohiyama, M., and Muraoka, N., 2004. Damage Detection from High-resolution Satellite Images for the 2003 Boumerdes, Algeria Earthquake, *Proceedings of the 13th World Conference on Earthquake Engineering*, CD-ROM, Paper No. 2595, 13p.
- Yamazaki, F., Matsuoka, M., Warnitchai, P., Polngam, S., and Ghosh, S., 2005. Tsunami Reconnaissance Survey in Thailand Using Satellite Images and GPS, *Asian Journal of Geoinformatics*, Vol. 5, No. 2, pp. 53-61.
- Yano, Y., Yamazaki, F., Matsuoka, M., and Vu, T., T., 2004. Building Damage Detection of the 2003 Bam, Iran Earthquake using QuickBird Images, *Proceedings of the 25th Asian Conference on Remote Sensing*, pp. 618-623.